Hydrodynamic Analysis of a High-Speed Marine Towed System

D.E. Calkins*
Systems Exploration, Inc., San Diego, Calif.

The objective of this work was to develop a general model of a marine towed system and to verify its accuracy by comparison with full-scale towed system measurements. Unlike other computer cable models, this model comprises a representation of both the towed body and towline. The model is completely general in that it will predict the steady-state three-dimensional behavior of the towed system in either a rectangular (straight ahead towing) or cylindrical (steady turn) coordinate system. Fully instrumented trials of a full-scale towed system provided data for correlation with the model. The results of the correlation study indicate that the model is capable of predicting the behavior (towed body orientation and forces, and towline spatial configuration and tension distribution) of the towed system with engineering accuracy.

Nomenclature

Vectors

$\bar{a}$ = acceleration
$\bar{r}$ = radius
$\bar{T}_0$ = tension at body
$\bar{U}$ = velocity
$\bar{\omega}$ = angular velocity

Towed Body

A_w = wing area, ft^2
b_w = wing span, ft
B = buoyancy, lb
C_w = mean wing chord, ft
F_h, M_h = hydrodynamic damping force and moment, lb and ft-lb
$F_{\dot{h}}, M_{\dot{h}}$ = hydrodynamic added mass force and moment, lb and ft-lb
l = length, ft
k_1 = roll angle control system gain, deg/deg
k_2 = roll rate control system gain, deg s/deg
$I_{x,y,z}$ = moments of inertia, ft-lb s^2
J_{xz} = polar moment of inertia, ft-lb s^2
M_b = mass, lb s^2/ft
R_b = turn radius, ft
U_b = velocity, fps
W = weight, lb
X_b, Z_b = distance from towpoint to buoyancy center, ft
X_h, Z_h = distance from towpoint to hydrodynamic center, ft
X_w, Z_w = distance from towpoint to mass center, ft
β = sideslip angle, deg ($-\psi$)
δ_e = elevator deflection, deg
δ_r = rudder deflection, deg
Θ = pitch angle, deg
ϕ = roll angle, deg
ψ = yaw angle, deg

Towline

c = chord, ft
c_r = drag coefficient
f_{am} = added mass hydrodynamic force, lb/ft
f_n = normal hydrodynamic force, lb/ft
f_s = lateral hydrodynamic force, lb/ft
f_t = tangential hydrodynamic force, lb/ft
f_w = net weight in water, lb/ft
m = mass/ft , lb s^2/ft^2
R_t = drag at $\phi_t = 90$ deg, lb/ft
T = tension, lb
t = thickness, ft
μ_{ij} = added mass coefficient

Towcraft

U_0 = velocity, fps
$\dot{\Psi}$ = turn rate, deg/s

Subscripts

b = towed body
s = towcraft
t = towline

Received March 23, 1977; revision received Aug. 24, 1978.

Index categories: Marine Mooring Systems and Cable Mechanics; Marine Vessel Systems, Submerged and Surface.
*Head, Ocean Systems Dept. Member AIAA.

Introduction

MANY applications exist for a high-speed marine towed system in conjunction with advanced technology marine vehicles such as hydrofoils and Surface Effect Ships. The U.S. Navy has developed a "testbed" towed system to study and identify the hydromechanical problems of high-speed towing. Here a towed system comprises a towline, either a bare or faired cable, or an integrally faired towline, and a towed body. Towing trials[1-5] were conducted aboard the U.S. Navy Hydrofoil Highpoint, Fig. 1, where stable towing, with an immersed scope of 400 ft, was demonstrated to a speed of 42 knots with a body depth of 324 ft and turn rates up to 4 deg/s.

Concurrently with the system hardware development, a three-dimensional steady-state digital computer simulation of the towed system was developed. The purpose of the simulation was to provide a general purpose tool which could predict the steady-state behavior of the towed system with engineering accuracy. This model has subsequently been updated and refined to increase its computational capability. The purpose of this work is to present the results of a correlation study which compares the output of the simulation with measured data from the towing trials.

Towed System Description

Towline

The integrally faired towline, which is shown in Fig. 2, consists of four individual elements: 1) an S-glass/epoxy resin molded strength member, 2) a flexible chlorosulfonated polyethylene rubber aft fairing, 3) two RG-58U coaxial electrical conductors, and 4) a protective rubber impregnated Dacron outer covering. The towline was molded into a streamlined NACA 63-A022 shape by a process which allowed a continuous 600-ft length to be fabricated.

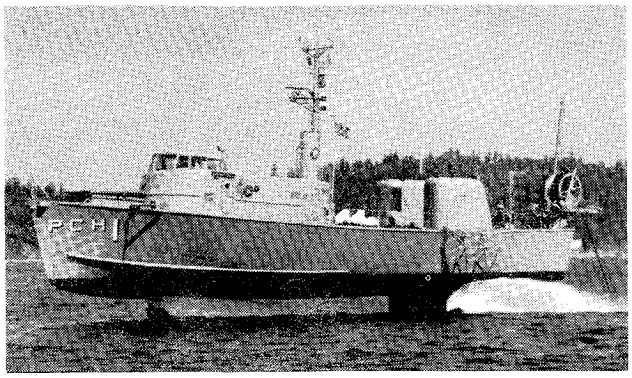

Fig. 1 PCH-1 (highpoint): towing at 42 knots and a depth of 324 ft.

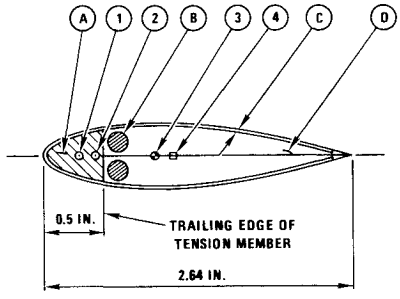

	ITEM	POSITION (PERCENT CHORD)
1.	CENTER OF TENSION	11.8
2.	SHEAR CENTER	16.8
3.	CENTER OF GRAVITY	35.6
4.	CENTER OF BUOYANCY	41.0

	ITEM	AREA ($IN.^2$)	MODULUS OF ELASTICITY (P. S. I.)
A.	STRENGTH MEMBER	0.15	9.4×10^6
B.	COAXIAL CABLES	0.03	0.51×10^6
C.	FABRIC COVERING	0.11	0.003×10^6
D.	RUBBER FAIRING	0.71	0.003×10^6

SECTION: NACA 63A022
WEIGHT (AIR): 0.707 LB/FT
WEIGHT (WATER): 0.269 LB/FT
ULTIMATE TENSION: 31,150 LB.
WORKING TENSION: 10,000LB.

Fig. 2 Integrally faired towline.

Towed Body

The towed body, or depressor, Fig. 3, served to provide a downforce at the lower towline termination, and a housing for the required instrumentation. The body was dynamically depressed with a wing, and therefore required an automatic control system for yaw and roll positioning control. Depth position and roll attitude were provided by two servo loops contained in the control system. The roll control servo loop actuated the rudder on the vertical stabilizer to control the body roll angle in accordance with a commanded roll angle. The roll control system operated in a closed-loop mode driven by roll and roll rate gyro signals. The second servo loop accuated the elevators on the horizontal stabilizer to vary pitch angle, and, consequently, the depth of the body. The elevator control loop was operated in an open-loop mode.

Towed System Trials – Measured Data

A total of 17 measurands were sensed and recorded to provide a complete characterization of the towed system performance.[6,7] These are listed in Table 1 in terms of their position either at the upper end of the towline at the towcraft, or at the lower end at the towed body. Also listed are the type of instrumentation used, the range of the measurand, and its accuracy both in terms of absolute limits and percent of full-scale range.

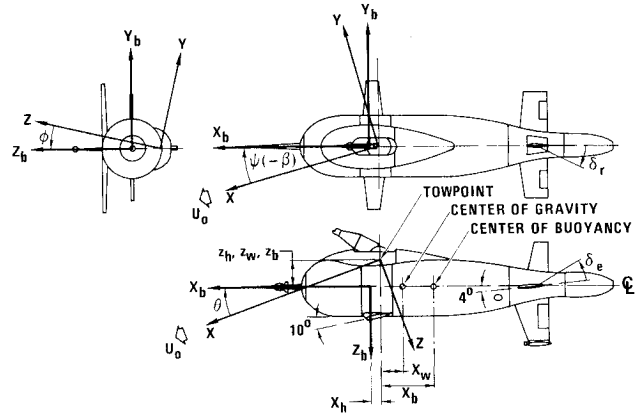

PRINCIPAL (BODY) AXES- X_b, Y_b, Z_b
STABILITY AXES- X, Y, Z

SPECIFICATIONS		
A_w	WING AREA, FT^2	2.28
C_w	MEAN AERODYNAMIC CHORD, FT	0.63
W_A	WEIGHT, LB (AIR)	1051
W_w	WEIGHT, LB (WATER)	446
B	BUOYANCY, LB	605
l	L. O. A., FT	9.76
d	DIAMETER, FT	1.83
b_w	WINGSPAN, FT	3.65
	NACA 0012 TAIL SECTIONS	
	NACA 0015 WING SECTION	

Fig. 3 Towed body outboard profile.

Computer Simulation

The simulation comprises two distinct mathematical models to represent the towed system. The first is a linearized characterization of the towed body which provides the lower tension vector and body orientation, or boundary condition of the towline. The second model is a nonlinear continuum representation of the towline which provides its tension distribution and spatial configuration.

Towed Body Mathematical Model

Three right-hand orthogonal coordinate systems are used in developing the towed body equations of steady motion. These are: 1) a principal axis (X_b, Y_b, Z_b) system located with the X_b axis lying along the longitudinal centerline and the Z_b axis down through the quarter chord of the wing mean chord, 2) a stability axis (X, Y, Z) system with its origin at the towpoint and the X axis aligned with the steady-state velocity vector $\bar{U}$, and 3) an inertial system (X_e, Y_e, Z_e). Steady horizontal flight is assumed so that the Z axis may be assumed to be aligned with gravity. These coordinate systems are shown in Fig. 4.

Under the assumption of steady state and small angular deviations from the mean equilibrium position, the equations of steady motion may be linearized by making the small angle assumption. Although a condition of steady state exists, a constant acceleration vector $\bar{a}$ will exist in the case of a steady-state turn. Towcraft speed, turnrate, and elevator deflection are independent variables, while body pitch, roll, yaw, rudder deflection, and towline tension vector, which acts at the towpoint, are the dependent variables.

The body equations of steady motion may be derived by equating the external forces acting on the body with the time rate of change of the momentum, and the external moments with the time rate of change of the moment of momentum (angular momentum) with respect to inertial space. The towpoint is assumed to allow no moment transfer, hence the equations of steady motion in the principal axis system may

Table 1 Towing trials measurands

No.	Measurand	How measured	Range	Accuracy	Accuracy, % full-scale range
(A)	Measurands at towcraft				
1	Winch pitch	Vertical gyro	±15 deg	±0.25 deg	±0.833
2	Winch roll	Vertical gyro	±15 deg	±1.0 deg	±3.33
3	Winch azimuth	Potentiometer	±69 deg	±1.0 deg	±0.833
4	Towline depression angle	Potentiometer	20-90 deg	±1.0 deg	±1.43
5	Towline fleet angle	Potentiometer	±10 deg	±333 lb	±5.00
6	Upper tension	Load cell	0-10,000 lb	±333 lb	±3.33
7	Immersed towline scope	Marks on towline	200-400 ft	±0.5 ft	±0.25
(B)	Measurands at towed body				
8	Towstaff pitch	Potentiometer	35-70 deg	±1.0 deg	±1.43
9	Towstaff roll	Potentiometer	±8.5 deg	±0.75 deg	±4.40
10	Lower tension	Load cell	10,000 lb	±400 lb	±4.00
11	Depth	Pitot tube/static pressure	0-500 ft	±6 ft	±1.2
12	Speed	Pitot tube/differential pressure	0-76 fps	±0.48 fps	±0.63
13	Depressor pitch	Vertical gyro	±10 deg	±0.6 deg	±3.00
14	Depressor roll	Vertical gyro	±30 deg	±1.0 deg	±1.67
15	Elevator angle	Potentiometer	0-25 deg	±0.5 deg	±2.00
16	Rudder angle	Potentiometer	±12.5 deg	±0.5 deg	±2.00
17	Yaw rate	Rate gyro	0-5 deg/s	±0.25 deg/s	±5.00

be written as two vector equations:

Summation of Forces at Towpoint

$$\Sigma F=\frac{\mathrm{d}(M\bar{U})}{\mathrm{d}t}=M_b\left[\frac{\mathrm{d}\bar{U}}{\mathrm{d}t}+\bar{\omega}\times\bar{U}\right] \tag{1}$$

but $\mathrm{d}\bar{U}/\mathrm{d}t=0$, therefore,

$$\bar{W}+\bar{B}+\bar{F}_h+\bar{F}_{\dot{h}}+\bar{T}_0=\bar{M}_b(\bar{\omega}\times\bar{U})=M_b\bar{a} \tag{2}$$

Summation of Moments at Towpoint

$$\Sigma\bar{M}+(\bar{a}\times M_b\bar{r}_w)=\frac{\mathrm{d}\bar{H}}{\mathrm{d}t}=\frac{\partial\bar{H}}{\partial t}+\bar{\omega}\times\bar{H} \tag{3}$$

where $\bar{H}$ is the moment of momentum about towpoint. Since $\partial\bar{H}/\partial t=0$, then

$$\bar{M}_w+\bar{M}_B+\bar{M}_h+\bar{M}_{\dot{h}}+(\bar{a}\times M_b\bar{r}_w)=\bar{\omega}\times\bar{H} \tag{4}$$

The term $\bar{a}\times M_b\bar{r}_w$ exists since moments are taken about the towpoint rather than the body center of mass. A control equation is necessary if the towed body has a control system

$$\delta_r=k_1\phi+k_2\dot{\phi} \tag{5}$$

A vector in the stability axis system may be transformed into the principal axis system by a sequence of rotation of the Euler angles of β, θ, ϕ. Thus,

$$\begin{Bmatrix}X_b\\Y_b\\Z_b\end{Bmatrix}=[A]\begin{Bmatrix}X\\Y\\Z\end{Bmatrix}=\left[\begin{array}{c|c|c}\cos\beta\cos\theta & -\sin\beta\cos\theta & -\sin\theta\\ \hline \cos\beta\sin\theta\sin\phi+\sin\beta\cos\phi & \cos\beta\cos\phi-\sin\beta\sin\theta\sin\phi & \cos\theta\sin\phi\\ \hline \cos\beta\sin\theta\cos\phi-\sin\beta\sin\phi & -\sin\beta\sin\theta\cos\phi-\cos\beta\sin\phi & \cos\theta\cos\phi\end{array}\right]\begin{Bmatrix}X\\Y\\Z\end{Bmatrix} \tag{6}$$

Making the small angle approximation, A reduces to

$$[A]=\left[\begin{array}{c|c|c}1 & -\beta & -\theta\\ \hline \beta & 1 & \phi\\ \hline \theta & -\phi & 1\end{array}\right]$$

The linear and angular velocity vectors are then

$$\bar{U}=[A]\begin{Bmatrix}U_b\\0\\0\end{Bmatrix}=U_b[i+\beta j+\theta k] \tag{7}$$

$$\bar{\omega}=[A]\begin{Bmatrix}0\\0\\\dot{\Psi}\end{Bmatrix}=\dot{\Psi}[-\theta i+\phi j+k] \tag{8}$$

thus

$$\bar{a}=\bar{\omega}\times\bar{U}=U_b\dot{\Psi}[-\beta i+j-\phi k] \tag{9}$$

The radius vector to the center of mass is

$$\bar{r}_w=X_w i+Z_w k \tag{10}$$

therefore,

$$\bar{a}\times M_b\bar{r}_w=M_bU_b\dot{\Psi}[Z_w i+(Z_w\beta-X_w\phi)j-X_w k] \tag{11}$$

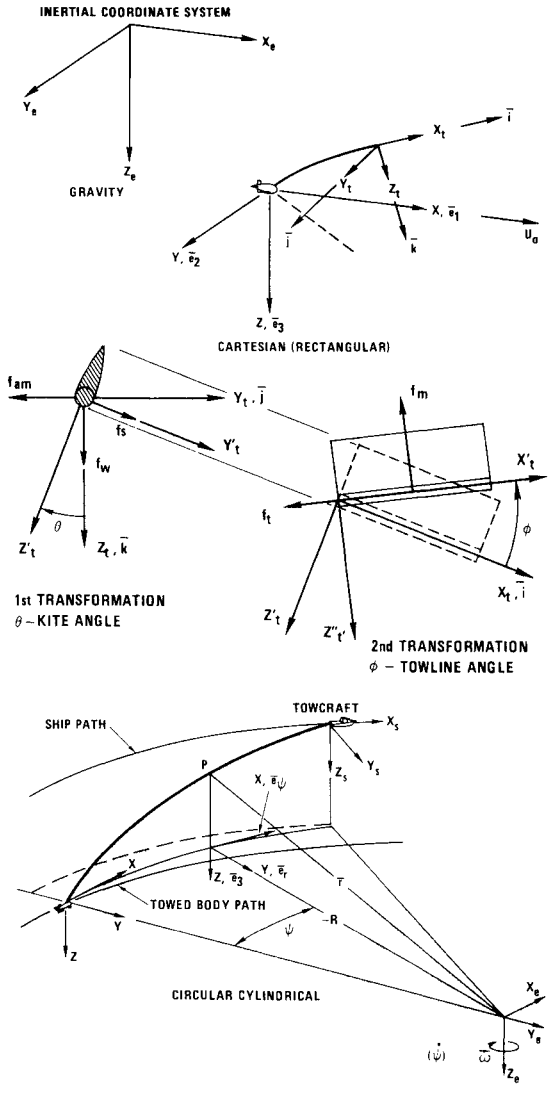

Fig. 4 Towed system coordinate systems.

Now, since,

$$\bar{H}=\bar{r}_w\times(\bar{\omega}\times\bar{r}_w)\,dm$$
$$=\dot{\Psi}[(-\theta I_x-J_{xz})i+(\phi I_y)j+(I_z+\theta J_{xz})k] \tag{12}$$

where

$$I_x=(I_x)_{cg}+M_b(Z_w)^2$$
$$I_y=(I_y)_{cg}+M_b(\sqrt{X_w{}^2+Z_w{}^2})^2$$
$$I_z=(I_z)_{cg}+M_b(X_w)^2$$

then

$$\bar{\omega}\times H=\dot{\Psi}^2\{[(I_z-I_y)\phi]i+[(I_z-I_x)\theta-J_{xz}]j+[J_{xz}\phi]k\} \tag{13}$$

The gravitational and buoyancy moments are

$$\bar{M}_w=\bar{r}_w\times\bar{W}\quad\text{and}\quad\bar{M}_B=\bar{r}_w\times\bar{B} \tag{14}$$

where

$$\bar{W}=[A]\begin{Bmatrix}0\\0\\W\end{Bmatrix}=W[-\theta i+\phi j+k]$$

$$\bar{B}=[A]\begin{Bmatrix}0\\0\\B\end{Bmatrix}=B[-\theta i+\phi j+k]$$

Therefore,

$$M_w=W[(-Z_w\phi)i-(Z_w\theta+X_w)j+(X_w\phi)k] \tag{15a}$$

$$\bar{M}_B=B[(-Z_b\phi)i-(Z_b\theta+X_b)j+(X_b\phi)k] \tag{15b}$$

The hydrodynamic forces and moments are

$$\bar{M}_h=\bar{M}_{h_0}+\bar{r}_h\times\bar{F}_h \tag{16}$$

where

$$M_{h_0}=M_{x_h}i+M_{y_h}j+M_{z_h}k$$

and

$$\bar{F}_h=F_{x_h}i+F_{y_h}j+F_{z_h}k$$

thus,

$$\bar{M}_h=(M_{x_h}-F_{y_h}Z_h)i+(M_{y_h}+F_{x_h}Z_h-F_{z_h}X_h)j+(M_{z_h}+F_{y_h}X_h)k \tag{17}$$

where

$$F_{x_h}=\frac{\rho A_w}{2}\left[C_{x_0}+C_{x_\theta}\theta+C_{x_{\delta_e}}\delta_e\right]U_b^2$$

$$F_{y_h}=\frac{\rho A_w}{2}\left[C_{y_\beta}U_b^2\beta+\frac{b_w}{2}C_{y_r}U_b\dot{\Psi}-\frac{b_w}{2}C_{y_p}U_b\dot{\Psi}\theta+C_{y_{\delta_r}}U_b^2\delta_r\right]$$

$$F_{z_h}=\frac{\rho A_w}{2}\left[(C_{z_0}+C_{z_\theta}\theta)U_b^2+\frac{C_w}{2}C_{z_q}U_b\dot{\Psi}\phi+C_{z_{\delta_e}}U_b^2\delta_e\right]$$

$$M_{x_h}=\frac{\rho A_w b_w}{2}\left[C_{l_\beta}U_b^2\beta+\frac{U_b\dot{\Psi}b_w}{2}(C_{l_r}+C_{l_p}\theta)+C_{l_{\delta_r}}U_b^2\delta_r\right]$$

$$M_{y_h}=\frac{\rho A_w C_w}{2}\left[(C_{M_0}+C_{M_\theta}\theta)U_b^2+\frac{C_w}{2}C_{M_q}U_b^2\dot{\Psi}\phi+C_{M_{\delta_e}}U_b^2\delta_e\right]$$

$$M_{z_h}=\frac{\rho A_w b_w}{2}\left[C_{n_\beta}U_b^2\beta+\frac{U_b\dot{\Psi}b_w}{2}(C_{n_r}-C_{n_p}\theta)+C_{n_{\delta_r}}U_b^2\delta r\right]$$

The control system equation becomes

$$\delta_r=k_1\phi+k_2\dot{\phi}=k_1\phi-k_2\dot{\Psi}\theta \tag{18}$$

The hydrodynamic added mass forces and moments are

$$\bar{M}_{\dot{h}}=\bar{r}_h\times\bar{F}_{\dot{h}} \tag{19}$$

where

$$\bar{F}_{\dot{h}}=F_{x_{\dot{h}}}i+F_{y_{\dot{h}}}j+F_{z_{\dot{h}}}k \qquad F_{x_{\dot{h}}}=-\frac{\rho l^3}{2}C_{x_{\dot{u}}}\beta U_b\dot{\Psi}$$

$$F_{y_{\dot{h}}}=\frac{\rho l^3}{2}C_{y_{\dot{v}}}U_b\dot{\Psi} \qquad F_{z_{\dot{h}}}=-\frac{\rho l^3}{2}C_{z_{\dot{w}}}\phi U_b\dot{\Psi}$$

Thus,

$$\bar{M}_{\dot{h}} = (-F_{y_{\dot{h}}} Z_h)\boldsymbol{i} + (F_{x_{\dot{h}}} Z_h - F_{z_{\dot{h}}} X_h)\boldsymbol{j} + F_{y_{\dot{h}}} X_h)\boldsymbol{k} = \frac{\rho l^3}{2} U_b \dot{\Psi}$$

$$\times \left[(-C_{y_{\dot{v}}} Z_h)\boldsymbol{i} + (-C_{x_{\dot{u}}} \beta Z_h + C_{z_w} \phi X_h)\boldsymbol{j} + (C_{y_{\dot{v}}} X_h)\boldsymbol{k} \right] \quad (20)$$

Equations (11, 13, 15, 17, 18, and 20) may be substituted into Eq. (4), and the coefficients of the three unknowns, ϕ, β, and θ, collected to give a solution of the form:

$$\bar{M} = (B_{11}\phi + B_{12}\beta + B_{13}\theta + C_1)\boldsymbol{i} + (B_{21}\phi + B_{22}\beta + B_{23}\theta + C_2)\boldsymbol{j}$$

$$+ (B_{31}\phi + B_{32}\beta + B_{33}\theta + C_3)\boldsymbol{k} = 0 \quad (21)$$

thus

$$[B] \begin{Bmatrix} \phi \\ \beta \\ \theta \end{Bmatrix} = \begin{Bmatrix} -C_1 \\ -C_2 \\ -C_3 \end{Bmatrix}$$

so that

$$\begin{Bmatrix} \phi \\ \beta \\ \theta \end{Bmatrix} = [B]^{-1} \begin{Bmatrix} -C_1 \\ -C_2 \\ -C_3 \end{Bmatrix} \quad (22)$$

Equation (2) may now be rewritten to obtain the towline tension vector acting on the body:

$$T_0 = M_b \bar{a} - \bar{W} - \bar{B} - \bar{F}_h - \bar{F}_{\dot{h}} = T'_x \boldsymbol{i} + T'_y \boldsymbol{j} + T'_z \boldsymbol{k} \quad (23)$$

where $\bar{T}_0$ is the towline tension vector acting the body with components defined in the body principal axis system. Substituting, we have

$$T'_x = -M_b U_b \dot{\Psi}\beta + (W+B)\theta - F_{x_h} - F_{x_{\dot{h}}} \quad (24)$$

$$T'_y = M_b U_b \dot{\Psi} - (W+B)\phi - F_{y_h} - F_{y_{\dot{h}}} \quad (25)$$

$$T'_z = M_b U_b \dot{\Psi}\phi - W - B - F_{z_h} - F_{z_{\dot{h}}} \quad (26)$$

For the towline simulation, the components in the stability axis system are needed; hence,

$$\begin{Bmatrix} T_x \\ T_y \\ T_z \end{Bmatrix} = [A]^{-1} \begin{Bmatrix} T'_x \\ T'_y \\ T'_z \end{Bmatrix} = \begin{Bmatrix} T'_x + T'_y\beta + T'_z\theta \\ -T'_x\beta + T'_y - T'_z\phi \\ -T'_x\theta + T'_y + T'_z \end{Bmatrix}$$

and

$$\bar{T}_0 = T_x \bar{e}_1 + T_y \bar{e}_2 + T_z \bar{e}_3 \quad (27)$$

Towline Mathematical Model

Three-dimensional steady-state models of towlines in the past have either been developed in a Cartesian coordinate system to handle the straight towing case, or in a circular cylindrical coordinate system to handle the steady turn case, for example, see Wang,[8] and Choo and Casarella.[9] The model developed in this work is completely general in that it is capable of handling all of the following cases: 1) straight towing (in-plane), two-dimensional; 2) straight towing (out-of-plane), three-dimensional, including either or both side forces on the towline or towed body; 3) steady turn, three-dimensional; and 4) steady turn, three-dimensional, including either or both sideforces on the towline or towed body.

The towline is assumed to be continuous, inextensible, flexible ($EI_x \equiv EI_y \equiv GJ \equiv 0$), and uniform in density and geometry along its length. A mathematical model of the towline capable of handling both straight towing and steady turn configurations requires equations of steady motion in both Cartesian and circular cylindrical coordinate systems.

The first is a stability axis (X, Y, Z) system which is fixed in and moving with the towed body and is colinear with a second system (X_s, Y_s, Z_s) which is fixed and moving with the towcraft, Fig. 4. For the case of the straight tow, a principal axis system (X_l, Y_l, Z_l), Fig. 4, is fixed within the towline such that the X_l axis is the tangent vector to the towline along its length. The radius vector to a point P on the towline is

$$\bar{r} = X\bar{e}_1 + Y\bar{e}_2 + Z\bar{e}_3 \quad (28)$$

For an inextensible towline

$$\bar{\imath} = \frac{\partial \bar{r}}{\partial S} = \frac{dX}{dS}\bar{e}_1 + \frac{dY}{dS}\bar{e}_2 + \frac{dZ}{dS}\bar{e}_2 = \frac{d\bar{r}}{dS} \quad (29)$$

since

$$\frac{d\bar{e}_1}{dS} \equiv \frac{d\bar{e}_2}{dS} \equiv \frac{d\bar{e}_3}{dS} \equiv 0$$

The towline angle ϕ is defined as the angle between the tangent vector $\bar{\imath}$ and the velocity vector $\bar{U}$, so that

$$\bar{\jmath} = \bar{U} \times \left[\frac{\bar{\imath}}{U \sin\phi} \right] \quad \text{and} \quad \bar{k} = \bar{\jmath} \times \bar{\imath} \quad (30)$$

The transformation of a vector in the (X, Y, Z) system to the (X_l, Y_l, Z_l) system, for an order of rotation of θ, ϕ is

$$\begin{Bmatrix} \bar{\imath} \\ \bar{\jmath} \\ \bar{k} \end{Bmatrix} = [A] \begin{Bmatrix} \bar{e}_1 \\ \bar{e}_2 \\ \bar{e}_3 \end{Bmatrix}$$

$$= \begin{bmatrix} \cos\phi & \sin\theta\sin\phi & -\cos\theta\sin\phi \\ 0 & \cos\theta & \sin\theta \\ \sin\theta & -\sin\theta\cos\phi & \cos\theta\cos\phi \end{bmatrix} \begin{Bmatrix} \bar{e}_1 \\ \bar{e}_2 \\ \bar{e}_3 \end{Bmatrix} \quad (31)$$

From Eq. (31)

$$\bar{\imath} = (\cos\phi)\bar{e}_1 + (\sin\theta\ \sin\phi)\bar{e}_2 - (\cos\theta\ \sin\phi)\bar{e}_3 \quad (32)$$

Therefore,

$$\frac{dX}{dS} = \cos\phi; \quad \frac{dY}{dS} = \sin\theta\ \sin\phi; \quad \frac{dZ}{dS} = -\cos\theta\ \sin\phi \quad (33)$$

are the directional derivatives in (X, Y, Z).

The second, a cylindrical coordinate system (Ψ, R, Z), Fig. 4, rotates with the ship about the Z_e axis, with unit vectors $\bar{e}_\Psi$, $\bar{e}_r$, and $\bar{e}_3$. The orientation of $\bar{e}_\Psi$ and $\bar{e}_r$ varies with S along the towline so that

$$\frac{d\bar{e}_r}{d\Psi} = \bar{e}_\Psi \qquad \frac{d\bar{e}_\Psi}{d\Psi} = -\bar{e}_r \quad (34)$$

Dividing by dS

$$\frac{d\bar{e}_r}{dS} = \bar{e}_\Psi \frac{d\Psi}{dS} \qquad \frac{d\bar{e}_\Psi}{dS} = -\bar{e}_r \frac{d\Psi}{dS} \quad (35)$$

Also, we have:

Position Vector

$$\bar{r} = -R\bar{e}_r - Z\bar{e}_3 \tag{36}$$

Angular Rate Vector

$$\bar{\omega} = \dot{\Psi}\bar{e}_3 \tag{37}$$

Velocity Vector

$$\bar{U} = \bar{\omega} \times \bar{r} = (R\dot{\Psi})\bar{e}_\Psi \tag{38}$$

Acceleration Vector

$$\frac{\partial \bar{U}}{\partial t} = \bar{U} \times \bar{\omega} = (R\dot{\Psi}^2)\bar{e}_r \tag{39}$$

Since $\bar{i} = d\bar{r}/dS$, then $\bar{i} = (\cos\phi)\bar{e}_\Psi + (\sin\theta \sin\phi)\bar{e}_r$

$$-(\cos\theta \sin\phi)\bar{e}_3 = -R\frac{d\bar{e}_r}{dS} - \bar{e}_r\frac{dR}{dS} - \bar{e}_3\frac{dZ}{dS} \tag{40}$$

Substituting Eq. (34) into Eq. (39), then,

$$\frac{d\Psi}{dS} = -\frac{\cos\phi}{R} \qquad \frac{dR}{dS} = -\sin\theta \sin\phi$$

$$\frac{dZ}{dS} = -\cos\theta \sin\phi \tag{41}$$

are the directional derivatives in (Ψ, R, Z).

The towline equation of motion in the rectangular coordinate system is

$$m\left(\frac{\partial \bar{U}}{\partial t}\right) = 0 = \frac{\partial T\bar{i}}{\partial S} + f_w\bar{e}_3 - f_t\bar{i} + f_s\bar{j} - f_n\bar{k} \tag{42}$$

where

$$\frac{\partial T\bar{i}}{\partial S} = T\left(\frac{d\bar{i}}{dS}\right) + \bar{i}\left(\frac{dT}{dS}\right)$$

and

$$\frac{d\bar{i}}{dS} = \left(\sin\phi\frac{d\theta}{dS}\right)\bar{j} - \left(\frac{d\phi}{dS}\right)\bar{k} \tag{43}$$

The normal and tangential hydrodynamic forces, f_n and f_t, may be defined in terms of loading functions which are functions of ϕ only, $[f_n/R_t = f_n(\phi)$ and $f_t/R_t = f_t(\phi)]$, where R_t is the drag at $\phi = 90$ deg

$$R_t = C_r \tfrac{1}{2}\rho U^2 t \tag{44}$$

The hydrodynamic sideforce is

$$f_s = C_y \tfrac{1}{2}\rho U^2 C \tag{45}$$

Substituting Eq. (43) into Eq. (42), and rearranging, we have

$$\frac{dT}{dS} = f_w \sin\phi \cos\theta + f_t \tag{46a}$$

$$\frac{d\theta}{dS} = \frac{-f_w \sin\theta - f_s}{T \sin\phi} \tag{46b}$$

$$\frac{d\phi}{dS} = \frac{f_w \cos\phi \cos\theta - f_n}{T} \tag{46c}$$

The equation of motion in the cylindrical coordinate system is modified from Eq. (42) by the addition of an added mass term, f_{am}, to account for the steady acceleration, thus,

$$m\frac{\partial \bar{U}}{\partial t} = (mR\dot{\Psi}^2)\bar{e}_r = \frac{\partial T\bar{i}}{\partial S} + f_w\bar{e}_3 - f_t\bar{i} + f_s\bar{j} - f_n\bar{k} + f_{am}\bar{e}_r \tag{47}$$

where

$$f_{am} = -(\mu_{ij}m)\frac{\partial \bar{U}}{\partial t} = -(\mu_{ij}mR\dot{\Psi}^2)\bar{e}_r \tag{48}$$

Again, after the proper substitutions

$$\frac{dT}{dS} = f_w \sin\phi \cos\theta + f_t + mR\dot{\Psi}^2(1 + \mu_{11})\sin\phi \sin\theta \tag{49a}$$

$$\frac{d\theta}{dS} = \frac{[mR\dot{\Psi}^2(1 + \mu_{21}) - (T/R)\cos^2\phi]\cos\theta - f_w\sin\theta - f_s}{T\sin\phi} \tag{49b}$$

$$\frac{d\phi}{dS} = \frac{[mR\dot{\Psi}^2(1 + \mu_{33}) - (T/R)]\cos\phi \sin\theta + f_w \cos\phi \cos\theta - f_n}{T} \tag{49c}$$

We thus have six simultaneous nonlinear O.D.E.'s, Eqs. (33) and (46), or Eqs. (41) and (49), for the towline equations of motion. A fourth order Runge-Kutta numerical routine is used in the program to integrate these equations. For the steady turn case, the turn radius of the towed body is not known, since it is the boundary conditions at the ship $(\dot{\Psi}, U_0)$ that are typically specified. In order to initiate the solution of problem, the velocity of the towed body is assumed equal to that of the ship, $U_b = U_0$. After the first pass through the towline program, the body turn radius R_d is computed using the final radius vector of the towline. The body velocity is then $U_b = R_b\dot{\Psi}$. The iteration procedure is repeated until the change in body turn radius is within a prescribed tolerance. After the integration of the equations is complete, a coor-

Table 2 Towed body input data

Characteristics		Longitudinal plane coefficients		Lateral plane coefficients	
A_w	= 2.28 ft^2	C_{x_0}	= −0.165	C_{y_β}	= −2.74/rad
b_w	= 3.65 ft	C_{x_θ}	= −1.78/rad	C_{y_p}	= 1.17/rad
C_w	= 0.63 ft	$C_{x_{\delta_e}}$	= 0./rad	C_{y_r}	= 6.64/rad
l	= 7.82 ft	C_{z_0}	= 0.70	$C_{y_{\delta_r}}$	= −0.223/rad
I_x	= 26.3 ft-lb-s^2	C_{z_θ}	= −5.16/rad	C_{l_β}	= 1.5/rad
I_y	= 282.3 ft-lb-s^2	C_{z_q}	= −43.4/rad	C_{l_p}	= −0.888/rad
I_z	= 285.7 ft-lb-s^2	$C_{z_{\delta_e}}$	= 0.581/rad	C_{l_r}	= −1.72/rad
J_{x_z}	= 0.0 ft-lb-s^2	C_{M_0}	= 1.15	$C_{l_{\delta_r}}$	= 0.067/rad
M_b	= 42.0 lb-s^2/ft	C_{M_θ}	= −16.4/rad	C_{n_β}	= 1.125/rad
W	= 1051.0 lb	C_{M_q}	= −676/rad	C_{n_p}	= −1.67/rad
B	= −605.0 lb	$C_{M_{\delta_e}}$	= 4.46/rad	C_{n_r}	= −6.55/rad
X_w	= −0.74 ft	$C_{x_{\dot{u}}}$	= −0.0049	$C_{n_{\delta_r}}$	= 0.288/rad
Z_w	= 0.92 ft	$C_{z_{\dot{w}}}$	= −0.0779	$C_{y_{\dot{v}}}$	= 0.0615/rad
X_b	= −1.03 ft				
Z_b	= 0.92 ft				
X_h	= 0.25 ft				
Z_h	= 0.86 ft				
k_1	= 1.0 deg/deg				
k_2	= 0.75 deg/deg/s				

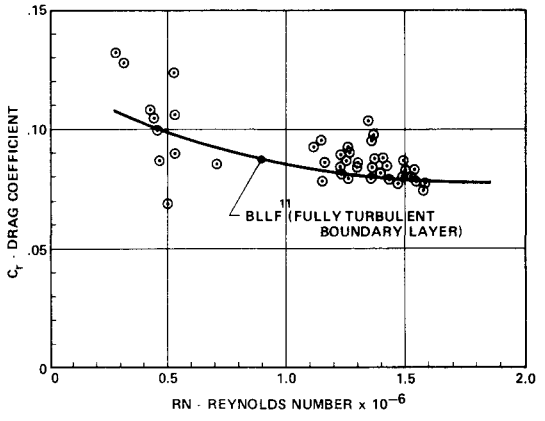

Fig. 5 Towline drag coefficient.

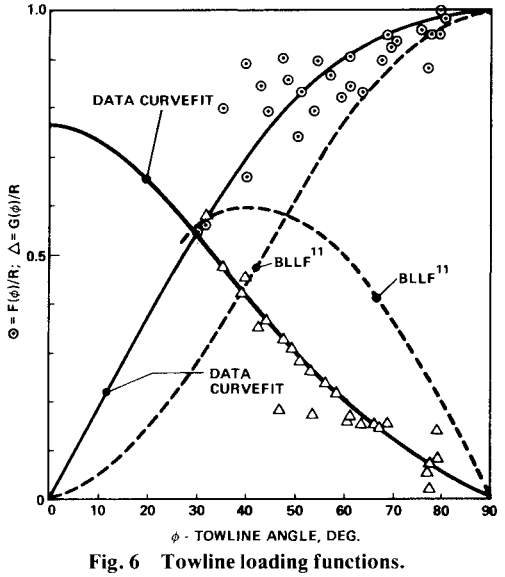

Fig. 6 Towline loading functions.

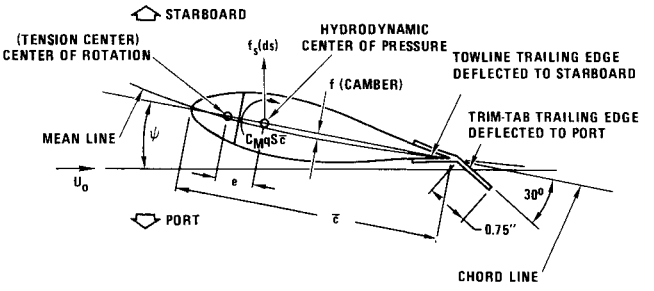

Fig. 7 Cambered towline moment balance.

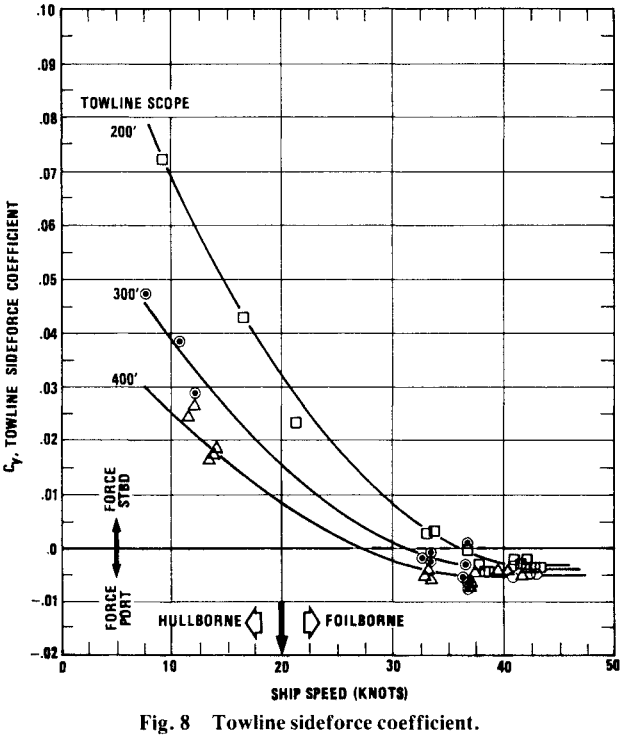

Fig. 8 Towline sideforce coefficient.

dinate transformation is used to transform the towline spatial configuration from the X, Y, Z into the X_s, Y_s, Z_s system, thus allowing a direct comparison of the simulation output with measured trials data.

Simulation Inputs

Towed Body

The towed body hydrodynamic coefficients were originally computed theoretically,[10] however, as the trials data were analyzed, it became evident that certain of the coefficients required correcting.[4] The simulation inputs for the towed body including its geometrical, inertial and hydrodynamic characteristics are listed in Table 2.

Added Mass

The towline section was assumed to be a flat plate for the purpose of computing the added mass coefficients, thus

$$\mu_{11} \equiv \mu_{33} \equiv 0; \quad \text{and} \quad \mu_{22} = \rho \pi c^2/4m \tag{50}$$

Drag Coefficient

A theoretical analysis for determining the hydrodynamic forces on a faired towline based on boundary layer theory[11] predicted the drag coefficient for the NACA 63A002 section as a function of Reynold's number assuming a turbulent boundary layer. In addition, amethod was developed for computing the drag coefficient from the measured towing trials data. These data, shown for immersed scopes of 200, 300, and 400 ft, are compared to the theoretical curve in Fig. 5. The theoretical curve, which is seen to approximate closely the mean of the data was used as the input to the simulation.

Loading Functions

The boundary-layer analysis[11] was also used to estimate the normal and tangential loading functions (BLLF) for the NACA 63A022 section. Loading functions, which were also developed from the trials data using the towline equations of motion,[3] are compared to the theoretical curves in Fig. 6. The agreement with the mean of the trials data is seen to be poor. Ramsey[12] has shown that the loading functions are periodic and can be expressed in terms of a Fourier Series with $f_n(\phi)$ containing only the odd terms of a sine series and $f_t(\phi)$ containing only the odd terms of a cosine series. The loading functions used as the simulation input were obtained by curve fitting the mean of the trials data, so that

$$f_n(\phi)/R_t = 1.04 \sin\phi + 0.0334 \sin 3\phi - 0.0083 \sin 5\phi \tag{51a}$$

$$f_t(\phi)/R_t = 0.6332 \cos\phi + 0.1246 \cos 3\phi + 0.0132 \cos 5\phi \tag{51b}$$

Sideforce Coefficient

During the conduct of towline trials, it was found that the towline developed a substantial sideforce so that out-of-plane configurations, termed kiting, resulted. After consideration of several postulations as to the cause of the kiting, one was identified as the most probable. This was the presence of a

Table 3 Towcraft run configurations

Case	Run no.	U_0(kt)	δ_e(deg)	$\dot{\Psi}$(deg/s)	
1	039-A-21	40.9	−5.8	0.0	
2	039-A-A	40.0	−5.8	3.1	(starboard turn)
3	039-A-37	41.5	−9.7	0.0	
4	039-A-B	39.3	−9.7	−4.3	(port turn)

small amount of asymmetry (camber) in the towline section distributed along the length of the towline. Accurate section coordinate measurements were taken at 14 stations along the length of the towline. After plotting on an enlarged scale, it was determined that an average deflection of the section mean line, f, of 0.0065 in. existed. Based on a section chord length of 2.64 in., this is a camber ratio, f/c, of 0.0025. Because of this camber, it was postulated that the towline would assume a yaw angle to the flow in order to balance out the moments about its longitudinal tension axis, resulting in a sideforce which, in turn, was responsible for the kiting of the towed system.

To remedy this problem during the towing trials, small metal trim tabs (0.75 in. by 1.5 in.), deflected to counteract the yawing moment due to the camber, were attached at 10-ft intervals along the length of the towline. This procedure, although undesirable from a towed system development standpoint, allowed the deployment of up to the desired maximum of 400 ft of towline. The hypothesized yaw moment balance situation of the towline section is depicted in Fig. 7. An estimate of the sideforce coefficient based on the measured camber ratio of 0.0025 resulted in a value of 0.055. This corresponds to a sideforce coefficient of an unloaded section.

A data analysis procedure was developed which computed an average sideforce coefficient from the measured trials data.[3] This analysis assumed that the camber, and hence the sideforce coefficient, was constant along the length of the towline. The data, presented in Fig. 8 for immersed scopes of 200, 300, and 400 ft, show that the averaged sideforce coefficient varies with both speed and immersed scope. One possible explanation for both of these variations is as follows. The camber is, in fact, not constant over the length of the towline. Consequently, the variation with immersed scope might be expected. The variation with speed is possibly explained by noting that the aft 80% of the towline section is of a flexible rubber material. As the speed increases, this aft portion may deform, thus unloading the section and relieving the camber. At the higher foilborne speeds, the negative sideforce coefficient may be due then to the residual effect of the metal trim tabs which are not totally relieved. This whole problem will require further detailed research. The mean of the data was used as the input to the simulation.

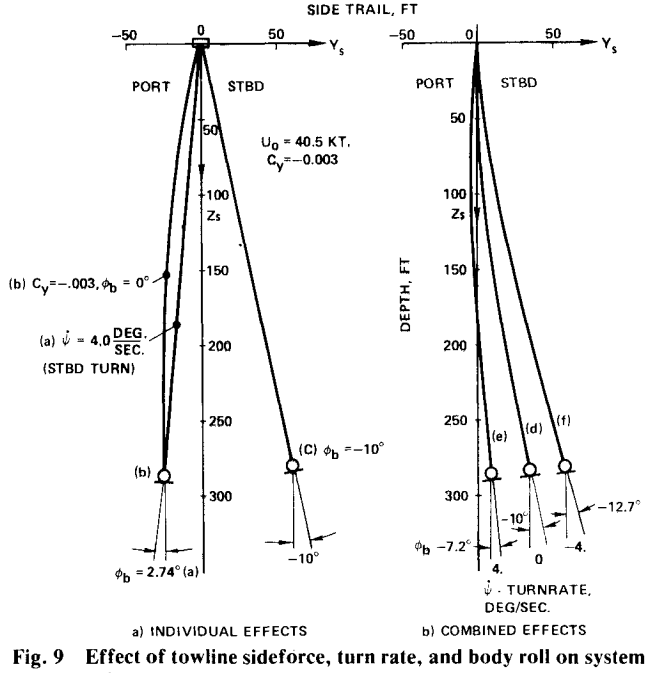

Fig. 9 Effect of towline sideforce, turn rate, and body roll on system configuration.

Discussion

Data from four towcraft runs, representing examples of both straight runs and turns to port and starboard, were selected for correlation purposes. These run configurations are presented in Table 3.

To counteract the towline sideforce during the trials, the towed body active roll control system was used to roll the body providing a counteracting sideforce to the towline sideforce such that the towline entered the water with no kite angle evident at the surface. Thus, the body was not directly astern of the towcraft centerline.

In order to provide insight into the independent effects of turnrate, towline sideforce, and body roll angle, three test cases were run and are shown in Fig. 9. It is seen that a positive turnrate (turn to starboard), $\dot{\Psi}=4.0$ deg/s, causes kiting to port in the ship coordinate system, (a). The centrifugal force induced on the body by the turnrate is seen to roll the body starboard wing down at an angle of 2.74 deg. A negative (to port) towline sideforce, $c_y=-0.003$, causes kiting to port relative to the ship, (b), while the body roll remains at zero. Rolling the body port wing down (negative), $\phi_b=-10$ deg, causes kiting to starboard (c). The effect of adding the three variables is also shown in Fig. 9 in sequence. Adding the towline sideforce and body roll, (d), is seen to

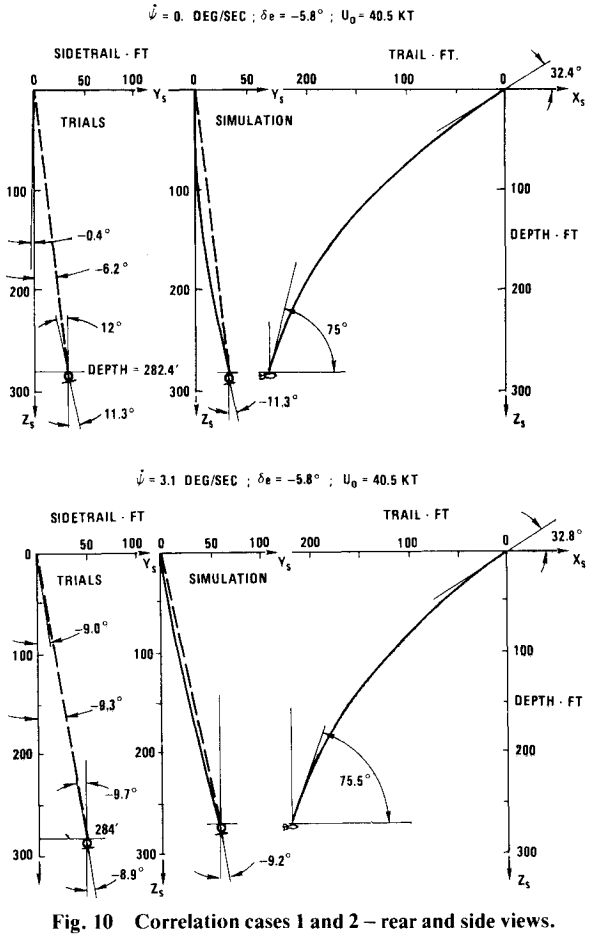

Fig. 10 Correlation cases 1 and 2 – rear and side views.

Table 4 Comparison of trials data and simulation

Item	Case 1 Trials	Case 1 Simulation (% diff.)	Case 2 Trials	Case 2 Simulation (% diff.)	Case 3 Trials	Case 3 Simulation (% diff.)	Case 4 Trials	Case 4 Simulation (% diff.)
Lower tension, lb	6940	6952. (+0.2)	6955	6559. (+10.1)	7950	7370. (−7.3)	8507	8390. (−1.4)
Upper tension, lb	8928	9362. (+4.9)	7887	8814. (+11.8)	10163	9550. (−6.0)	10659	10659. (0.)
Lower towline angle, deg	75.0	75.0 (0.)	75.5	70.0 (−7.3)	76.0	73.5 (−3.3)	35.4	35.5 (+0.3)
Upper towline angle, deg	32.4	34.0 (+6.3)	32.8	35.5 (+8.2)	36.6	36.0 (−1.6)	76.2	74.0 (+2.9)
Lower kite angle, deg	12.0	11.3 (−5.8)	−9.7	−10. (−3.1)	−14.7	−17. (−7.9)	−22.6	−18 (+20.4)
Upper kite angle, deg	−0.4	−4.0 (−950)	−9.0	−16. (−77.8)	−2.7	0. (+100.)	15.1	12.0 (+20.4)
Body depth, ft	282.4	288. (+2.0)	284.	272. (−4.2)	305.5	296. (−3.1)	302.	288. (−4.6)
Body pitch, deg	1.1	0.7 (−36.4)	1.5	0.6 (−6.0)	0.5	−0.3 (−160)	0.8	−0.3 (−137.5)
Body roll, deg	−11.3	−11.3 (0.)	−8.9	−9.2 (+3.4)	−14.2	−14.2 (0.)	−22.4	−17. (+24.)

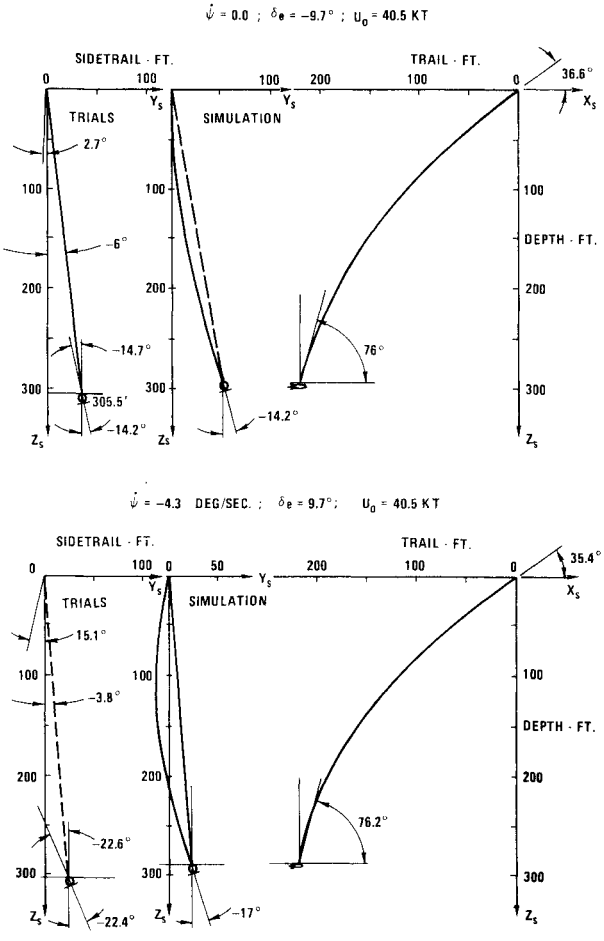

Fig. 11 Correlation cases 3 and 4 – rear and side views.

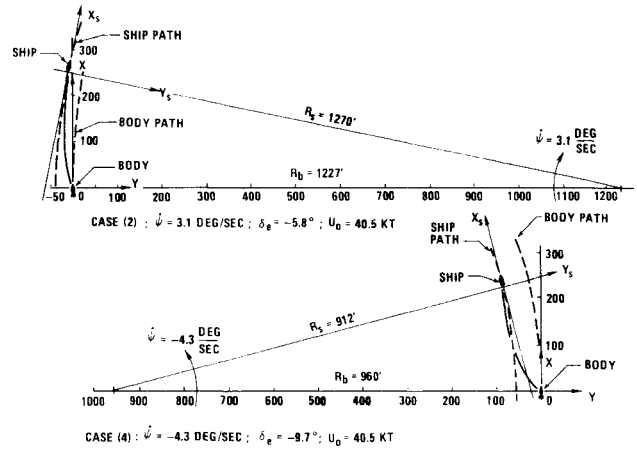

Fig. 12 Correlation cases 2 and 4 – plan views.

result in a configuration that exhibits a zero kite angle at the surface. The effect of a turn to starboard, (e), $\dot{\Psi} = 4$ deg/s, causes the system kiting to decrease, while a turn to port, $\dot{\Psi} = -4$ deg/s, causes an increase in kiting, (f).

For the four comparison cases, values of c_r and c_y from Figs. 5 and 8 were used along with an averaged speed of 40.5 knots and the actual values of commanded body roll. It should be noted that the commanded body roll was set during straight towing, and not altered during the turns. Changes in body roll during a turn are due to its centrifugal force. The sequence of the cases is a straight run, (1), a turn to starboard, (2), followed by a change in the towed body elevator angle which increases the depth, another straight run, (3), and finally a turn to port, (4). Profile and rear views of the towed system configuration for all four cases, in addition to plan views for the two turn cases, are presented in Figs. 10-12. The plan view of cases (2) and (4), Fig. 12, shows the transformation from the body to the ship coordinate system.

A comparison of the simulation output with the trials data is made in Table 4 for selected measurands. It should be noted that the towline and kite angle are the projections on the X_sZ_s and Y_sZ_s planes, respectively. The percent difference between the two is also tabulated. With the exceptions of the upper kite angle and the towed body pitch, all differences are within ±15%. Differences in the lower towline tensions are between ±15%, while this same difference exists for the upper tensions, which indicates that the computed values of C_{x_0} and C_{z_0} used in the body simulation are low and should be revised.

Conclusions

Overall, the ability of the simulation to predict the steady behavior of this type of towed system in straight running and in turns within ±15% has been verified. Taking into account the accuracy of the trials data and the problems of the simulation input data, the model is within acceptable engineering standards.

References

[1] Calkins, D.E., "Hydrofoil High-Speed Towed System Trial Evaluation – Part I: Summary and Data," Naval Undersea Center, San Diego, Calif., TP 241, Aug. 1972.

[2] Calkins, D.E. and Ford, L.A., "Hydrofoil High-Speed Towed System Trial Evaluation – Part II: System Description and Operational Critique," Naval Undersea Center, San Diego, Calif., TP 241, Aug. 1972.

[3]Calkins, D.E., "Hydrofoil High-Speed Towed System Trial Evaluation – Part III: Towline Hydrodynamic Performance," Naval Undersea Center, San Diego, Calif., TP 241, Aug. 1972.

[4]Calkins, D.E. and Benz, R.C., "Hydrofoil High-Speed Towed System Trial Evaluation – Part IV: Depressor Hydrodynamic Performance," Naval Undersea Center, San Diego, Calif., TP 241, Aug. 1972.

[5]Calkins, D.E. and Tunstall, E.B., "Hydrofoil High-Speed Towed System Trial Evaluation – Part V: Computer Simulation Correlation," Naval Undersea Center, San Diego., Calif., TP 241, Aug. 1972.

[6]"Data Reduction Support for PCH-1 Towed Trials," General Dynamics/Convair, San Diego, Calif., Rept. No. 6 DC-BKF 70-001B, May 1977.

[7]"Towing Trials Summary Report PCH-1," Boeing Co., Seattle, Wash., Doc. D2-133703-54-1 and 2, May 1971.

[8]Wang, H.T., "A FORTRAN IV Program for the Three-Dimensional Steady-State Configuration of Extensible Flexible Cable Systems," NSRDC Rept. 4384, Sept. 1974.

[9]Choo, Y. and Casarella, M.J., "Configuration of a Towline Attached to a Vehicle Moving in a Circular Path," *Journal of Hydronautics,* Vol. 6, Jan. 1972, pp. 51-57.

[10]"Computation of the Hydrodynamic Coefficients of the Hydrospace Research Corporation Towed Body," Bendix Corp., Dept. No. SR 69-11, Feb. 1969.

[11]Calkins, D.E., "Faired Towline Hydrodynamics," *Journal of Hydronautics,* Vol. 4, July 1970, pp. 113-119.

[12]Ramsey, J.P. and Dillon, D.B., "Emperical Hydrodynamic Characterization of Two Bare Double Armored Towlines," Hydrospace Research Corp., Rockville, Md., TR 293, Nov. 1971.